frontiers in Physics

BRIEF RESEARCH REPORT
published: 20 August 2021
doi: 10.3389/fphy.2021.727934

Dual Negative Differential of Heat Generation in a Strongly Correlated Quantum Dot Side-Coupled to Majorana Bound States

Zhu-Hua Wang and Wen-Cheng Huang*

College of Physics and Electromechanics, Fujian Longyan University, Longyan, China

We study theoretically the properties of local heat originated from energy exchange between electrons passing through a quantum dot (QD) coupled to a phonon bath. The dot is sandwiched between two normal metal leads and also side-coupled to Majorana bound states (MBSs) formed at opposite ends of a topological superconductor nanowire. We find that in addition to the negative differential of heat generation (NDHG) in the Coulomb blockade regime, another NDHG emerges near the leads' Fermi level due to the dot-MBS coupling. This dual NDHG effect is robust against the variation of intradot Coulomb interaction strength, and disappears if the QD is coupled to regular Fermions. Direct hybridization between the MBSs reduces their impacts on the electronic transport processes, and eliminates the dual NDHG effect. Our results show that the dual NDHG effect is quite efficient for inferring the existence of MBSs, and may remedy some limitations of the detection schemes relying on tunneling spectroscopy technique.

Keywords: heat current, electron-phonon interaction, majorana fermions, quantum dot, negative differential heat generation

OPEN ACCESS

Edited by:
Feng Chi,
Zhongshan Institute, China

Reviewed by:
Yingjie Chen,
Qufu Normal University, China
Lian-Liang Sun,
North China University of Technology, China

****Correspondence:***
Zhu-Hua Wang
lywzh666@163.com

Specialty section:
This article was submitted to Optics and Photonics, a section of the journal Frontiers in Physics

Received: *20 June 2021*
Accepted: *12 July 2021*
Published: *20 August 2021*

Citation:
Wang Z-H and Huang W-C (2021) Dual Negative Differential of Heat Generation in a Strongly Correlated Quantum Dot Side-Coupled to Majorana Bound States. Front. Phys. 9:727934. doi: 10.3389/fphy.2021.727934

1 INTRODUCTION

Majorana bound states (MBSs) are zero energy quasi-particles of Majorana fermions typically formed in low-dimensional topological superconductors [1, 2]. They obey non-Abelian statistics and can serve as anyons whose braiding can be used for constructing elementary logic gates for quantum computation [3–6]. Such a kind of logic gate depends only on the topology of the braiding path, and then small imperfections in the braiding are tolerable on the condition that the manipulations are topologically equivalent. Correspondingly, MBSs have been extensively investigated in the past decades as a prominent candidate for fault-tolerant topological quantum computation [7]. In addition, the MBSs are also promising in spintronics and thermoelectric effects. For example, the MBSs will strengthen the intrinsic π phase difference between spin-triplet pairings in Josephson junction [8]. Such a *π-phase shift* is demonstrated to induce a spin-dependent superconducting phase, i.e., spin-phase that is adjustable with the help of electric gates and the coupling energy between MBSs. This effect suggests an all-electrical spin control scheme and can also be used to manipulate and detect the MBSs [8]. If the electron-hole symmetry property of the MBSs is broken (e.g. by side-coupling one mode of the MBSs to a quantum dot (QD)) [9], the sign of the thermopower, which measures the generated bias voltage in response to a temperature difference applied at different ends of the system, can be reversed by changing the hybridization amplitude between the QD and the MBS [10, 11], or direct coupling between the MBSs [12, 13].

Moreover, the magnitude of the thermopower or thermoelectric efficiency can be significantly enhanced due to the existence of the MBSs [12, 13]. These results are useful in designing thermoelectric devices or detecting MBSs.

Experimentally, topological superconductors have been successfully realized in heterostructures comprised of a one-dimensional semiconductor nanowire having strong Rashba spin-orbit interaction and a proximitizing s-wave superconductor [1, 2, 14, 15]. With the help of a strong external magnetic field, the phase of the heterostructure can be driven into topological superconductor one and thus enable the formation of MBSs at opposite ends of the nanowire. As for the detection of MBSs, the most efficient scheme is the tunneling spectroscopy in Majorana nanowires sandwiched between normal metal leads. The MBSs will manifest itself by a zero-bias anomalous conductance peak [15]. Since this anomalous peak in the electric conductance may also originate from other reasons, such as the Kondo effect [16], anti-localization [17] and subgap states [18], some other detection schemes for the MBSs were then continuingly put forward. For example, signatures of MBSs can be inferred from the sign change or abnormal enhancement of the thermopower as was indicated above [9–13]. The existence of the MBSs can be deduced by measuring the Majorana entropy of an initial equilibrium state of the system [19]. Generally, the Majorana entropy will be ruined even when the transport amplitude of one mode of the MBSs is significantly blockaded, which can be directly measured in experiments. To avoid the above general issues, Smirnov very recently proposed to adjust the tunneling phases of one mode of the MBSs to bring out the universal Majorana plateau. Meanwhile, an experimental scheme that is realizable within present techniques was also proposed to measure entropy of the MBSs [19]. Signatures induced by MBSs may also be deduced from transport phenomena such as the abnormal changes of the shot noise [20–22], quantum noise [23, 24], thermoelectric noise [25], sign change of the tunnel magnetoresistance [26], splitting of the photon-assisted subbands [27], etc.

In fact, due to the unique charge neutral and zero energy properties, the above detection schemes still come with great difficulties and it is not sure if the existence of the MBSs can be completely determined. Recently, impacts of electron-phonon interaction on the MBSs-assisted transport have been studied [28, 29]. This is triggered by two motivations: one is that the electron-phonon interaction will induce significant decoherence effects that will change the transport behaviors and roles in quantum computation [30]; the other is that the phonons will play important roles in Majorana-induced Andreev reflection processes [28]. With continuing improvement of nanofabrication techniques, the length of the device becomes smaller than that of electron-phonon scattering, and thus the electron-phonon interaction is the main cause of heat generation by electrical current [30–34]. With increasing integration density on a chip, the issue of generated heat becomes more and more vital [35]. If the waste heat can not be removed as quickly as possible, the chips may not function properly. As was demonstrated by Sun *et. al.* [31, 32], the behaviors of the heat generation in nanodevices are quite different from those in the usual macroscopic ones. The Joule heating law $Q = JV$ for the local heat power density, where J is current density and V is the bias voltage applied across the system, is violated. Electrons transporting through a QD may absorb energy from a phonon bath attached to it even at zero temperature [36]. In the presence of intradot Coulomb interaction, the magnitude of heat generation may be quite small even under a large current [32]. In the Coulomb blockade regime, the heat generation decreases although the current's amplitude is monotonously enhanced *for* increasing bias voltage, a phenomenon was named as negative differential of the heat generation (NDHG) [32]. The NDHG is very similar to the negative differential conductance effect unique in nanodevices, and is expected to play an important role in phonon engineering subjects. In our previous work, MBSs-mediated heat generation by electrical current in a QD without Coulomb interaction was investigated [37]. It was found that the magnitude of the heat generation and electrical current is sensitive to the existence of MBSs. Under some conditions, the heat generation and electrical current can be individually suppressed and enhanced by changing the dot-MBSs or MBS-MBS couplings, which is ideal for energy-saving instruments. In the present manuscript, we revisit the problem of heat generation by taking the intradot Coulomb interaction into consideration. We find that the MBSs will induce another NDHG in addition to that in the absence of MBSs, which is named as dual NDHG that can be used for inferring the existence of the MBSs.

2 MODEL AND METHODS

The system under investigation can be described by the following Hamiltonian ($\hbar = 1$) [28, 29, 31, 32, 37].

$$H = \sum_{k,\beta,\sigma} \varepsilon_{k\beta\sigma} c^{\dagger}_{k\beta\sigma} c_{k\beta\sigma} + [\varepsilon_d + \lambda_q (a^{\dagger} + a)] \sum_{\sigma} d^{\dagger}_{\sigma} d_{\sigma} + U d^{\dagger}_{\uparrow} d_{\uparrow} d^{\dagger}_{\downarrow} d_{\downarrow} + \omega_q a^{\dagger} a + \sum_{k,\beta,\sigma} (t_{k\beta} c^{\dagger}_{k\beta\sigma} d_{\sigma} + H.c) + H_{MBSs}, \tag{1}$$

where the first term in the right side of **Eq. 1** describes the β-th ($\beta = L/R$) lead with $c^{\dagger}_{k\beta\sigma}$ ($c_{k\beta\sigma}$) being the electron creation (annihilation) operator having momentum k, energy $\varepsilon_{k\beta\sigma}$ and spin σ. The second term is for electrons on the QD and their interaction *to* the phonon with strength λ_q. The operator $d^{\dagger}_{\sigma}$ (d_{σ}) creates (annihilates) an electron having quantized single energy level ε_d. $a^{\dagger}(a)$ is for the creation (annihilation) operator of a phonon with frequency ω_q. The third term in the right side of **Eq. 1** is for Coulomb interaction between electrons on the QD, and the fourth term denotes the single phonon mode. The fifth term describes overlapping between the QD and the leads with $t_{k\beta}$ being the matrix element. The last term in **Eq. 1** is for the MBSs and their coupling to the QD, [15, 37–39]

$$H_{MBSs} = i\delta_M \eta_1 \eta_2 + \lambda \sum_{\sigma} (d_{\sigma} - d^{\dagger}_{\sigma}) \eta_1, \tag{2}$$

where the operator $\eta_{1/2}$ denotes the two modes of the MBSs located at opposite ends of the nanowire. In the present paper, we consider that the QD is only coupled to one mode of the MBSs

with coupling amplitude λ. The quantity ε_M is the overlap strength between the MBSs. The Majorana operators follow $\{\eta_\alpha, \eta_\beta\} = 2\delta_{\alpha\beta}$ and $\eta_\alpha = \eta_\alpha^\dagger$. According to previous work, we replace the Majorana operators by the regular fermion via [15] $\eta_1 = (1/\sqrt{2})(f + f^\dagger)$, and $\eta_2 = (-i/\sqrt{2})(f - f^\dagger)$, the Hamiltonian H_{MBSs} then is given by.

$$H_{MBSs} = \varepsilon_M\left(f^\dagger f - \frac{1}{2}\right) + \frac{\lambda}{\sqrt{2}}\sum_\sigma (d_\sigma - d_\sigma^\dagger)(f + f^\dagger). \tag{3}$$

To decouple the electron-phonon interaction in **Eq. 1**, we next perform a canonical transformation, [28, 29, 31, 32, 37], $\tilde{H} = XHX^\dagger$ with $X = \exp[(\lambda_q/\omega_q)(a_q^\dagger - a_q)\sum_\sigma d_\sigma^\dagger d_\sigma]$, and then **Eq. 1** becomes.

$$\tilde{H} = \sum_{k,\beta,\sigma}\varepsilon_{k\beta\sigma}c_{k\beta\sigma}^\dagger c_{k\beta\sigma} + \tilde{\varepsilon}_d\sum_\sigma d_\sigma^\dagger d_\sigma + \sum_{k,\alpha,\sigma}(\tilde{t}_{k\beta}c_{k\alpha\sigma}^\dagger d_\sigma + H.c) + \tilde{H}_{MBSs}, \tag{4}$$

where the dot level is $\tilde{\varepsilon}_d = \varepsilon_d - g\omega_q$ and Coulomb interaction strength $\tilde{U} = U - 2g\omega_q$ with $g = (\lambda_q/\omega_q)^2$. The tunnelling amplitude $t_{k\beta}$ and the coupling strengths between the dot and MBSs λ are individually given by $t_{k\alpha} = t_{k\alpha}X$ and $\tilde{\lambda} = \lambda X$ with $X = \exp[-g(a^\dagger - a)]$ [28, 29]. The other quantities in $\tilde{H}_{MBSs}$ are the same as in **Eq. 3**. If $t_{k\alpha}$ and λ are weak as compared to λ_q, X can be replaced by the expectation value $< X > = \exp[-g(N_{ph} + 1/2)]$, in which $N_{ph} = 1/[\exp(\omega_q/k_BT_p) - 1]$ the phonon distribution function with T_p the phonon temperature [12, 13]. The heat generation $J_q(t) = \omega_q\langle da_q^\dagger(t)a_q(t)/dt\rangle$ in frequency space is written based on the Green's functions as the following form, [31]

$$J_q = \mathrm{Re}\omega_q\lambda_q^2\sum_\sigma\int\frac{d\varepsilon}{2\pi}\{\tilde{G}_\sigma^<(\varepsilon)\tilde{G}_\sigma^>(\bar{\varepsilon}) - 2N_{ph}[\tilde{G}_\sigma^>(\varepsilon)\tilde{G}_\sigma^a(\bar{\varepsilon}) + \tilde{G}_\sigma^r(\varepsilon)\tilde{G}_\sigma^>(\bar{\varepsilon})]\}, \tag{5}$$

where $\bar{\varepsilon} = \varepsilon - \omega_q$, and $\tilde{G}_\sigma^{r,a,<,>}(\varepsilon)$ are the electron retarded, advanced, lesser and greater Green's functions. The retarded Green's function $\tilde{G}_\sigma^r(\varepsilon)$ is calculated from **Eq. 4** by the equation of motion method as, [38, 39]

$$\tilde{G}_\sigma^r(\varepsilon) = \frac{1 + (1 - \tilde{\lambda}^4\tilde{K}\tilde{K}_U)\Pi_\sigma}{\varepsilon - \tilde{\varepsilon}_d - \Sigma_{0,M}^r + i\tilde{\Gamma}}. \tag{6}$$

where $\tilde{\Gamma} = (\tilde{\Gamma}_L + \tilde{\Gamma}_R)/2$, with $\tilde{\Gamma}_\beta = \exp[-g(2N_{ph} + 1)]\Gamma_\beta$ and $\Gamma_\beta = 2\pi|t_{k\beta}|^2\rho_\beta$, where ρ_β is the local density of states in lead β. The quantities $\Pi_\sigma = \tilde{U}n_{\bar{\sigma}}/(\varepsilon - \tilde{\varepsilon}_d - \tilde{U} - \Sigma_{1,M}^r + i\tilde{\Gamma})$, $\tilde{\varepsilon}_d - \tilde{\lambda}^2K + i\tilde{\Gamma})$, $\tilde{K}_U = K/(\varepsilon + \tilde{\varepsilon}_d + \tilde{U} - \tilde{\lambda}^2K + i\tilde{\Gamma})$, and $K = \varepsilon/(\varepsilon^2 - \delta_M^2)$. The advanced Green's function in the above equation is $\tilde{G}_\sigma^a(\varepsilon) = [\tilde{G}_\sigma^r(\varepsilon)]^*$, and the lesser (greater) one is $\tilde{G}_\sigma^{<(>)}(\varepsilon) = \tilde{G}_\sigma^r(\varepsilon)\tilde{\Sigma}^{<(>)}\tilde{G}_\sigma^a(\varepsilon)$, in which the self-energies are individually given by $\tilde{\Sigma}^< = i[\tilde{\Gamma}_Lf_L(\varepsilon) + \tilde{\Gamma}_Rf_R(\varepsilon)]$, and $\tilde{\Sigma}^> = -i\{\tilde{\Gamma}_L[1 - f_L(\varepsilon)] + \tilde{\Gamma}_R[1 - f_R(\varepsilon)]\}$ [31]. The Fermi distribution function is $f_\beta(\varepsilon) = 1/\{\exp[(\varepsilon - \mu_\beta)/k_BT_e] + 1\}$, with chemical potential μ_β. $G^r(\varepsilon)$ is related to $\tilde{G}^r(\varepsilon)$ by [31] $G_\sigma^r(\varepsilon) = \sum_{n=-\infty}^{n=\infty}L_n\{\tilde{G}_\sigma^r(\varepsilon - n\omega_q) + [\tilde{G}_\sigma^<(\varepsilon - n\omega_q) - \tilde{G}_\sigma^<(\varepsilon + n\omega_q)]/2\}$, and $\tilde{G}_\sigma^<(\varepsilon) = -2i\Gamma_Lf_L(\varepsilon) + \Gamma_Rf_R(\varepsilon)/(\Gamma_L + \Gamma_R)\mathrm{Im}\tilde{G}_\sigma^r(\varepsilon)$, where $L_n = \exp[-g(2N_{ph} + 1)]\exp(n\omega_q/2k_BT)I_n[2g\sqrt{2N_{ph}(N_{ph} + 1)}]$, with $I_n(x)$ the modified nth Bessel function. The occupation number is calculated self-consistently from $n_\sigma = -i\int d\varepsilon/2\pi G_\sigma^<(\varepsilon)$, and the spin-dependent electric current is obtained also by the Green's function as [7, 30] $J_e = -e\Gamma_L\Gamma_R/[2\pi h(\Gamma_L + \Gamma_R)]\sum_\sigma\int d\varepsilon[f_L(\varepsilon) - f_R(\varepsilon)]\mathrm{Im}G_\sigma^r(\varepsilon)$.

3 RESULTS AND DISCUSSION

In the following numerical calculations, we *choose* the phonon frequency $\omega_q \equiv 1$ as energy unit ($\hbar = 1$), and consider the case of the dot is symmetrically coupled to the left and right leads with $\tilde{\Gamma}_L = \tilde{\Gamma}_R = 0.1\omega_q$. The electron-phonon coupling strength is fixed as $\lambda_q = \omega_q$, and the temperatures of the electrons and phonons are $T_e = T_p = 0.02\omega_q$. The chemical potential of the right lead μ_R is set to be zero as the energy zero point, and the bias voltage is $eV = \mu_L$. **Figure 1** shows the total electrical current J_e and heat generation J_q varying with respect to the bias voltage when the QD is coupled to one of the *MBSs* with different strengths. For dot level $\tilde{\varepsilon}_d = 0$, the electrical current J_e in **Figure 1A** has two steps respectively around bias values of $eV = \tilde{\varepsilon}_d$ and $eV = \tilde{\varepsilon}_d + \tilde{U}$. Between these two steps, the current's line-shape shows the typical Coulomb blockade effect [32]. The origination of this effect can be explained as follows: in the absence of bias voltage, i.e., $\tilde{\varepsilon}_d = \mu_L = \mu_R$, *there are an equal number of electrons in the left and right leads tunnel through the QD in opposite directions, and then results in zero charge current. In the presence of bias voltage* $eV = \mu_L$, *there are more electrons in the left lead than the right one entering into the QD and then tunneling out to the right lead, so the current is positive. For even larger bias voltage, the electron occupation number in the QD increases since the electrons' probability of dwelling on the dot becomes larger.* Correspondingly, the probability of other electrons to enter into the dot becomes smaller, and then the current's magnitude will not increase further. As shown in **Figure 1A**, the current reaches a plateau when the bias voltage is $\tilde{\varepsilon}_d < eV < \tilde{\varepsilon}_d + \tilde{U}$ due to the so-called Coulomb blockade effect. When $eV > \tilde{\varepsilon}_d + \tilde{U}$, the QD level $\tilde{\varepsilon}_d + \tilde{U}$ enters into the transport window and then the current's magnitude increases again. At the bias voltages of $eV = \tilde{\varepsilon}_d$ and $\tilde{\varepsilon}_d + \tilde{U}$, the electrical differential conductance $G_{dif} = dJ_e/dV$ has two sharp peaks, but is zero when $\tilde{\varepsilon}_d < eV < \tilde{\varepsilon}_d + \tilde{U}$, which is not shown here. There are some small steps in the curves of J_q versus eV due to the electron-phonon interaction, by which the QD energy level is modified into $\tilde{\varepsilon}_d = \varepsilon_d - g\omega_q$ [31, 32]. Now electrons can transport through the system whenever the energy states $\tilde{\varepsilon}_d + n\omega_q$ or $\tilde{\varepsilon}_d - n\omega_q$ enter into the bias window, which results in an abrupt increase of the electrical current. *In the presence of QD-MBSs coupling* ($\tilde{\lambda} \neq 0$), *we find that the current near zero bias voltage is obviously changed, whereas that at relatively larger bias voltage is less influenced. This is because the MBSs are zero in energy and only exert impacts on the current around zero bias voltage, which is consistent with the results of zero bias anomaly of the conductance serving as evidence of the MBSs.* [17, 20].

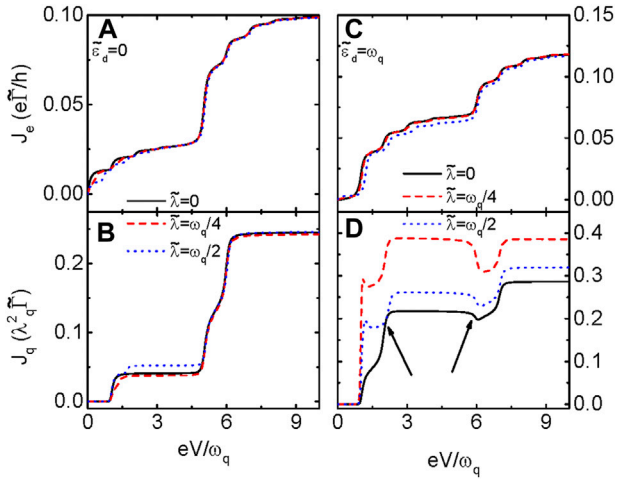

FIGURE 1 | Electrical current and heat generation varying with respective to the bias voltage when the QD is coupled to MBSs. **(A)** and **(B)** are for $\tilde{\varepsilon}_d = 0$ whereas $\tilde{\varepsilon}_d = \omega_q$ in **(C)** and **(D)**. The two arrows in **Figure 1D** indicate the two NDHG. The dot-MBSs coupling strength λ is set at different values. Other parameters are $\lambda_q = \omega_q$, $\tilde{\Gamma}_L = \tilde{\Gamma}_R = 0.1\omega_q$, $T_e = T_{ph} = 0.02\omega_q$, $\delta_M = 0$, $U = 5\omega_q$.

The line-shape of the heat generation in **Figure 1B** resembles that of the current influenced by the Coulomb blockade effect, but has no small steps induced by the electron-phonon interaction. The reason is that the heat generation in **Eq. 5** is calculated from the transformed Hamiltonian in which the electron and phonon is decoupled. Therefore, the plateaus in the heat generation are much flatter compared to those in the current. The heat generation has a delay of ω_q as compared to the electric current in **Figure 1A** [32]. This *is* because the heat generation J_q is caused by the phonon absorption and emission processes occurred between energy states ε and $\varepsilon \pm \omega_q$ [31, 32]. When the bias voltage is small $eV < \omega_q$, the electrons can not absorb enough energy from the external electrical field to emit phonon having energy $\hbar\omega_q$, and therefore the magnitude of the heat generation is zero. It is worth pointing out that this delay effect is absent in macroscopic systems and is more distinct at low temperature regimes. It emerges regardless of the existence of intradot Coulomb interaction or some other fields [31–34, 36]. In the presence of interaction between the MBSs *at the ends of a nanowire* ($\tilde{\lambda} \neq 0$), the magnitude of the electrical current in **Figure 1A** near the Fermi level $eV = 0$ is slightly decreased, with that at other bias voltage mainly remain unchanged which is indicated above. The heat generation in **Figure 1B**, however, can be either enhanced or suppressed. During the bias voltage of $\omega_q \leq eV \leq \tilde{U} + \omega_q$, the magnitude of the heat generation can be slightly enhanced for nonzero $\tilde{\lambda}$, but when $eV > \tilde{U} + \omega_q$ the magnitude of the heat generation is slightly suppressed.

When the dot level is tuned by gate voltage to be $\tilde{\varepsilon}_d = \omega_q$, positions of the steps in the current are changed accordingly (**Figure 1C**). The magnitude of the current changes more obviously by the dot-MBS coupling $\tilde{\lambda}$ as compared to the case of $\tilde{\varepsilon}_d = 0$ in **Figure 1A**. As found in Ref. [10], the electron transmission will become asymmetric for $\tilde{\varepsilon}_d \neq 0$ and develops a sharp peak at negative energy due to the dot-MBS coupling, which is out of the transport window. As a result of it, the current's magnitude is weakened for $\lambda \neq 0$. The line-shape of heat generation in **Figure 1D** is quite different from that in **Figure 1B**. First, the amplitude of the abrupt jump in heat generation at $eV = \tilde{\varepsilon}_d + \omega_q$ is much larger than that at $eV = \omega_q + \tilde{\varepsilon}_d + \tilde{U}$. This result is consistent with that in Ref. [32]. Second, in the absence of dot-MBS coupling, there is an obvious NDHG effect when the bias voltage is between $\tilde{\varepsilon}_d + \tilde{U} - \omega_q$ and $\tilde{\varepsilon}_d + \tilde{U}$, where the heat generation decreases with increasing bias voltage. This is because the electron passing through the QD can either absorb or emit a phonon. If the bias voltage V is between $\tilde{\varepsilon}_d + \tilde{U} - \omega_q$ and $\tilde{\varepsilon}_d + \tilde{U}$, the tunneling process can only be realized when the electron absorbs a phonon while electrons transport through the QD, inducing a NDHG. Third, we find in **Figure 1D** that another NDHG emerges when the bias voltage is between ω_q and $\omega_q + \lambda$ in the presence of dot-MBS hybridization, which is called dual NDHG in the present paper. The origination of the NDHG near ω_q is because the hybridization between the QD and MBS induces new states at $\tilde{\varepsilon}_d \pm \tilde{\lambda}$. Meanwhile, the NDHG in the Coulomb blockade regime is also enhanced by increasing $\tilde{\lambda}$. This enhanced and newly emerged NDHG can be used for deducing the existence of MBSs. We emphasize that the NDHG effect is more likely to emerge in the presence of intradot Coulomb interaction, as was shown in previous works [31, 32, 37].

To show the novel dual NDHG effect induced by the MBSs, we present the results when the dot is side-coupled to another QD serving as regular fermion in **Figure 2**. For the sake of notational consistency, we use the same symbols δ_M and $\tilde{\lambda}$ to individually denote the QD energy level and the coupling amplitude between the two dots. The Hamiltonian of the present system is given by $H_{MBSs} = \delta_M f^\dagger f + \tilde{\lambda}\sum_\sigma (f^\dagger d_\sigma + d_\sigma^\dagger f)$, and the Green's function is calculated as [40, 41]

$$\tilde{G}^r_\sigma(\varepsilon) = \frac{1 - n_{\bar{\sigma}}}{\varepsilon - \tilde{\varepsilon}_d - \Sigma^r_{1,M} + i\tilde{\Gamma}} + \frac{n_{\bar{\sigma}}}{\varepsilon - \tilde{\varepsilon}_d - \tilde{U} - \Sigma^r_{1,M} + i\tilde{\Gamma}}, \quad (7)$$

in which $\Sigma^r_{1,M} = \tilde{\lambda}^2/(\varepsilon - \delta_M)$. The molecular states of the structure of QD coupled to regular fermion are calculated

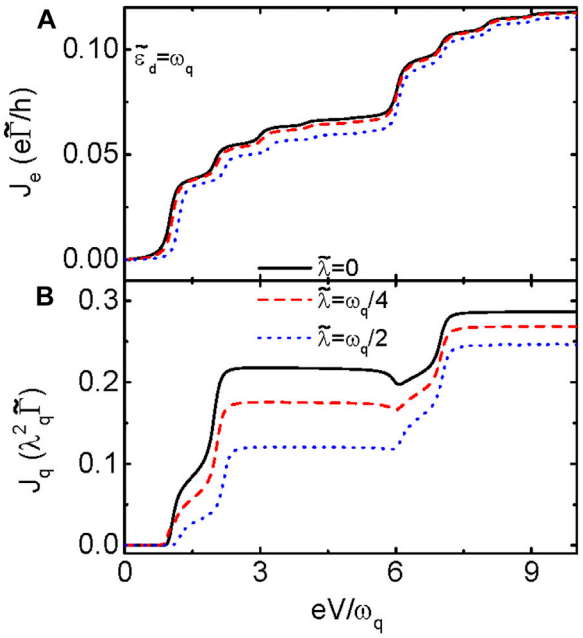

FIGURE 2 | J_e in **(A)** and J_q in **(B)** versus the bias voltage when the QD is coupled to regular fermions in another QD. As the present manuscript focuses on the NDHG occurred at non-zero dot level, here only the results of $\lambda_q = \omega_q$ is presented. Other parameters are the same to those in **Figure 2**.

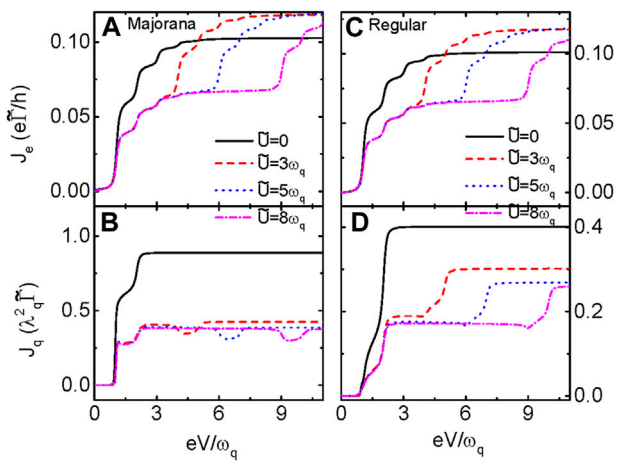

FIGURE 3 | (A) and **(B)** are individually for J_e and J_q in QD coupled to MBSs, and **(C)** and **(D)** are J_e and J_q in QD connected to regular fermions, respectively. The Coulomb interaction is chosen at different values with fixed $\lambda = \omega_q/4$. Other parameters are as in **Figure 2**.

from the above retarded Green's to be $\varepsilon = 0$ and $\varepsilon_{\pm} = (\delta_M \pm \sqrt{\delta_M^2 + 4\tilde{\lambda}^2})/2$, whereas those of the dot hybridized to MBSs are at $\varepsilon = 0$ and $\varepsilon_{\pm} = \pm\sqrt{\delta_M^2 + 2\tilde{\lambda}^2}$. Moreover, the phase shift of the two kinds of systems are different, [41] resulting in different behaviors of the current and heat generation in **Figure 2**. The electrical current in **Figure 2A** resembles that in **Figure 1C** only with changed positions of the steps, which indicates that the current is less influenced by the MBSs. The heat generation in **Figure 2B**, however, is very different from that in **Figure 1D**. Firstly, when the dot is coupled to regular fermion (another QD), the heat generation decreases with increasing $\tilde{\lambda}$ as shown in **Figure 2B**. But if the dot is coupled to MBS, the heat generation increases with increasing $\tilde{\lambda}$ which can be seen from **Figure 1D**. Secondly, the NDHG in the Coulomb blockade regime is eliminated by the stronger coupling between QD and regular fermion (**Figure 2B**), whereas that in QD-MBS structure is enhanced. Thirdly, the NDHG around $\omega_q + \tilde{\lambda}$ is also eliminated by increasing $\tilde{\lambda}$ when the QD is coupled to regular

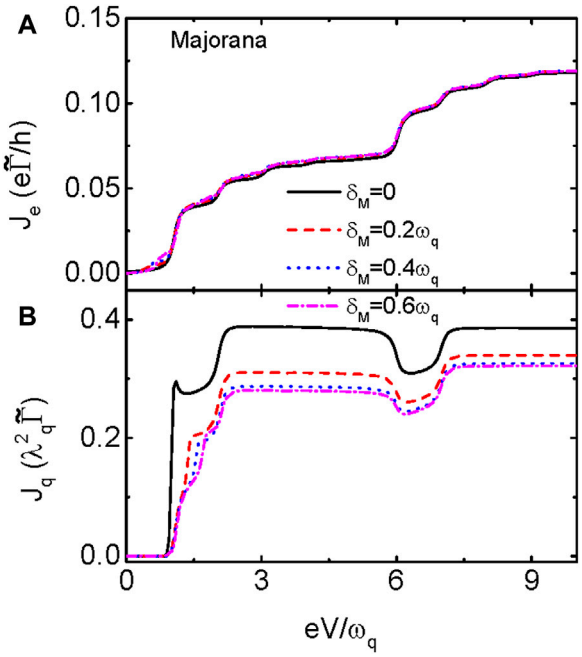

FIGURE 4 | J_e in **(A)** and J_q in **(B)** as functions of the bias voltage when the QD is coupled to MBSs for different values of δ_M and fixed. The Coulomb interaction is chosen at different values with fixed $\lambda = \omega_q/4$. Other parameters are as in **Figure 2**.

fermion given in **Figure 2B**. The above changes of the heat generation represents the unique properties of the MBSs as compared to those of the regular fermions, and then can be used for detection means for the MBSs. We have also calculated the case when the dot level is aligned to the Fermi level ($\tilde{\varepsilon}_d = 0$) and found that the phenomenon of NDHG disappears similar to the result in **Figure 1B**, and then we do not show them in the figure.

Figure 3 presents the impacts of different intradot Coulomb interaction on the electrical current and heat generation in both QD-MBS and QD-QD structures. The electrical current in **Figure 3A** when the dot is coupled to MBS shows small phonon-induced steps and plateaus. The intradot Coulomb interaction results in another plateau in higher voltage regimes and changes the strength of the current. The current in **Figure 3C** of QD-QD structure resembles that in **Figure 3A** and indicates the insufficiency of detecting MBS by transport means. The magnitude of the heat generation in **Figure 3B** for QD-MBS is decreased even for a weak $\tilde{U}$, and then almost *remains at* the same amount with further increasing $\tilde{U}$. Meanwhile, two NDHGs emerge as soon as the intradot Coulomb interaction is turned on. Further increase of the value of $\tilde{U}$ only changes the position of the NDHG in the Coulomb blockade regime, with the behavior at $eV = \omega_q + \tilde{\lambda}$ remains essentially unchanged. The heat generation in QD-QD structure, however, only has one NDHG in the Coulomb blockade regime. The above results show that the dual NDHG induced by MBS is quite robust against the variation of the amplitude of intradot Coulomb interaction.

Finally in **Figure 4**, we study the influences of direct hybridization between the MBSs δ_M, which is determined by the length and material properties of the nanowire, on the electrical current and heat generation when the QD is coupled to MBS. The case of the dot connected to another QD has been extensively studied [40], and we do not show it here. When the two modes of the MBSs are overlapped ($\delta_M \neq 0$), their impacts on the electrical current and heat generation is weakened. We find that the current in **Figure 4A** is slightly enhanced by increasing δ_M, with the positions of the steps and plateaus remaining unchanged. The magnitude of the heat generation, however, decreases in the presence of δ_M as shown in **Figure 4B**. The NDHG in the Coulomb blockade regime is almost unchanged by δ_M, whereas that near $\omega_q + \tilde{\lambda}$ is eliminated if the MBS-MBS coupling strength is large. The reason is that when the two modes of the MBSs interact with each other, they behave like regular fermions.

4 SUMMARY

In summary, we study properties of electric current and heat generation in a QD hybridized to one mode of MBSs prepared at the one end of a nanowire. Our results show that the properties of the electric current under the influence of MBS are quite similar to those when the dot is coupled to regular fermions. In the presence of intradot Coulomb interaction, the heat generation has a NDHG effect in the Coulomb blockade regime when there is no coupling between the QD and MBS. But another NDHG in lower bias voltage regime emerges, which is called the dual NDHG effect unique to the MBSs, when the dot interacts with the MBS. We find that the dual NDHG arises even for quite weak intradot Coulomb interaction and disappears if the MBS is replaced by

regular fermions. The overlap between the two modes of the MBSs destroys the dual NDHG effect, and reduces the magnitude of the electrical current because now the MBSs resemble regular fermions. The present results indicate that the behaviors of the heat current may be rather efficient for detecting the MBSs as compared to the pure electrical method.

DATA AVAILABILITY STATEMENT

The original contributions presented in the study are included in the article/supplementary material, further inquiries can be directed to the corresponding author.

AUTHOR CONTRIBUTIONS

Z-HW derived the formulae, performed partial numerical calculations, and wrote the original manuscipt. W-CH discussed the physical model, performed partial numerical calculations, and contributed in the paper writting.

FUNDING

This work was supported by Thirteenth five-year plan of educational science in Fujian province (Grant Nos. FJJKCG19-297 and 2019CG0707).

REFERENCES

1. Fu L, and Kane C. Superconducting Proximity Effect and Majorana Fermions at the Surface of a Topological Insulator. *Phys Rev Lett* (2008) 100:096407. doi:10.1103/PhysRevLett.100.096407
2. Qi X, and Zhang S. Topological Insulators and Superconductors. *Rev Mod Phys* (2011) 83:1057. doi:10.1103/RevModPhys.83.1057
3. Nayak C, Simon S, Stern A, Freedman M, and Sarma S. Non-abelian Anyons and Topological Quantum Computation. *Rev Mod Phys* (2008) 80:1083. doi:10.1103/RevModPhys.80.1083
4. Alicea J, Oreg Y, Refael G, von Oppen F, and Fisher M. Non-abelian Statistics and Topological Quantum Information Processing in 1d Wire Networks. *Nat Phys* (2011) 7:412. doi:10.1038/nphys1915
5. Karzig T, Knapp C, Lutchyn R, Bonderson P, Hastings M, Nayak C, et al. Scalable Designs for Quasiparticle-Poisoning-Protected Topological Quantum Computation with Majorana Zero Modes. *Phys Rev B* (2017) 95:235305. doi:10.1103/PhysRevB.95.235305
6. Huang H, Narozniak M, Liang F, Zhao Y, Castellano A, Gong M, et al. Emulating Quantum Teleportation of a Majorana Zero Mode Qubit. *Phys Rev Lett* (2021) 126:090502. doi:10.1103/PhysRevLett.126.090502
7. Karzig T, Cole W, and Pikulin D. Quasiparticle Poisoning of Majorana Qubits. *Phys Rev Lett* (2021) 126:057702. doi:10.1103/PhysRevLett.126.057702
8. Liu X, Li X, Deng D, Liu X, and Sarma S. Majorana Spintronics. *Phys Rev B* (2016) 94:014511. doi:10.1103/PhysRevB.94.014511
9. Hou C, Shtengel K, and Refael G. Thermopower and mott Formula for a Majorana Edge State. *Phys Rev B* (2013) 88:075304. doi:10.1103/PhysRevB.88.075304
10. López R, Lee M, Serra L, and Lim J. Thermoelectrical Detection of Majorana States. *Phys Rev B* (2014) 89:205418. doi:10.1103/PhysRevB.89.205418
11. Leijinse M. Thermoelectric Signatures of a Majorana Bound State Coupled to a Quantum Dot. *New J Phys* (2014) 16:015029. doi:10.1088/1367-2630/16/1/015029
12. Hong L, Chi F, Fu Z, Hou Y, Wang Z, Li K, et al. Large Enhancement of Thermoelectric Effect by Majorana Bound States Coupled to a Quantum Dot. *J Appl Phys* (2020) 127:124302. doi:10.1063/1.5125971
13. Chi F, Fu Z, Liu J, Li K, Wang Z, and Zhang P. Thermoelectric Effect in a Quantum Dot Side-Coupled to Majorana Bound States. *Nanoscale Res Lett* (2020) 15:79. doi:10.1186/s11671-020-03307-y
14. Mourik V, Zuo K, Frolov S, Plissard S, Bakkers E, and Kouwenhoven L. Signatures of Majorana Fermions in Hybrid Superconductor-Semiconductor Nanowire Devices. *Science* (2012) 336:1003. doi:10.1126/science.1222360
15. Liu D, and Baranger H. Detecting a Majorana-Fermion Zero Mode Using a Quantum Dot. *Phys Rev B* (2011) 84:201308. doi:10.1103/PhysRevB.84.201308
16. Wang R, Su W, Zhu J, Ting C, Li H, Chen C, et al. Kondo Signatures of a Quantum Magnetic Impurity in Topological Superconductors. *Phys Rev Lett* (2019) 122:1–6. doi:10.1103/PhysRevLett.122.087001
17. Pikulin D, Dahlhaus J, Wimmer M, Schomerus H, and Beenakker C. A Zero-Voltage Conductance Peak from Weak Antilocalization in a Majorana Nanowire. *New J Phys* (2012) 14:125011. doi:10.1088/1367-2630/14/12/125011
18. Kells G, Meidan D, and Brouwer P. Low-energy Subgap States in Multichannel P-Wave Superconducting Wires. *Phys Rev B* (2012) 85:060507. doi:10.1103/PhysRevB.85.060507
19. Smirnov S. Majorana Entropy Revival via Tunneling Phases. *Phys Rev B* (2021) 103:075440. doi:10.1103/PhysRevB.103.075440
20. Liu D, Cheng M, and Lutchyn R. Probing Majorana Physics in Quantum-Dot Shot-Noise Experiments. *Phys Rev B* (2015) 91:081405. doi:10.1103/PhysRevB.91.081405
21. Smirnov S. Non-equilibrium Majorana Fluctuations. *New J Phys* (2017) 19:063020. doi:10.1088/1367-2630/aa70a9
22. Bathellier D, Raymond L, Jonckheere T, Rech J, Zazunov A, and Martin T. Finite Frequency Noise in a normal Metal-Topological Superconductor junction. *Phys Rev B* (2019) 99:104502. doi:10.1103/PhysRevB.99.104502
23. Smirnov S. Majorana Finite-Frequency Nonequilibrium Quantum Noise. *Phys Rev B* (2019) 99:165427. doi:10.1103/PhysRevB.99.165427
24. Smirnov S. Dynamic Majorana Resonances and Universal Symmetry of Nonequilibrium Thermoelectric Quantum Noise. *Phys Rev B* (2019) 100:245410. doi:10.1103/PhysRevB.100.245410
25. Smirnov S. Universal Majorana Thermoelectric Noise. *Phys Rev B* (2018) 97:165434. doi:10.1103/PhysRevB.97.165434
26. Tang L, and Mao W. Detection of Majorana Bound States by Sign Change of the Tunnel Magnetoresistance in a Quantum Dot Coupled to Ferromagnetic Electrodes. *Front Phys* (2020) 8:147. doi:10.3389/fphy.2020.00147
27. Chi F, He T, Wang J, Fu Z, Liu L, Liu P, et al. Photon-assisted Transport through a Quantum Dot Side-Coupled to Majorana Bound States. *Front Phys* (2020) 8:254. doi:10.3389/fphy.2020.00254
28. Dai N, and Sun Q. Phonon-assisted Andreev Reflection at a Majorana Zero Mode. *Phys Rev B* (2019) 99:085436. doi:10.1103/PhysRevB.99.085436
29. Wang X, Wu B, Zhang S, Wang Q, and Gong W. Influences of Electron–Phonon Interaction on Quantum Transport through One Quantum-Dot System with Side-Coupled Majorana Zero Mode. *Ann Phys* (2020) 415:168127. doi:10.1016/j.aop.2020.168127
30. Li N, Ren J, Wang L, Zhang G, Hänggi P, and Li B. Colloquium: Phononics: Manipulating Heat Flow with Electronic Analogs and beyond. *Rev Mod Phys* (2012) 84:1045. doi:10.1103/RevModPhys.84.1045
31. Sun Q, and Xie X. Heat Generation by Electric Current in Mesoscopic Devices. *Phys Rev B* (2007) 75:155306. doi:10.1103/PhysRevB.75.155306
32. Liu J, Song J, Sun Q, and Xie X. Electric-current-induced Heat Generation in a Strongly Interacting Quantum Dot in the Coulomb Blockade Regime. *Phys Rev B* (2009) 79:161309. doi:10.1103/PhysRevB.79.161309
33. Chi F, Zheng J, Liu Y, and Guo Y. Refrigeration Effect in a Single-Level Quantum Dot with thermal Bias. *Appl Phys Lett* (2012) 100:233106. doi:10.1063/1.4720093
34. Chi F, and Sun L. Photon-assisted Heat Generation by Electric Current in a Quantum Dot Attached to Ferromagnetic Leads. *Chin Phys Lett* (2016) 33:117201. doi:10.1088/0256-307X/33/11/117201
35. Lebedev A, and Vinokur V. Heat Generation Due to the anderson Catastrophe in Mesoscopic Devices. *Phys Rev B* (2020) 102:195111. doi:10.1103/PhysRevB.102.195111
36. Pei W, and Sun Q. Time-averaged Heat Generation in a Quantum Dot Driven by an Alternating Current Bias. *J Appl Phys* (2012) 112:124306. doi:10.1063/1.4769804

37. Wang Z. Heat Generation by Electrical Current in a Quantum Dot Hybridized to Majorana Nanowires. *Front Phys* (2021) 9:704493. doi:10.3389/fphy.2021.704493
38. Stefański P. Properties of the Majorana-State Tunneling Josephson junction Mediated by an Interacting Quantum Dot. *J Phys Condens Matter* (2019) 31:185301. doi:10.1088/1361-648X/ab052a
39. Ricco L, de Souza M, Figueria M, Shelykh I, and Seridonio A. Spin-dependent Zero-Bias Peak in a Hybrid Nanowire-Quantum Dot System: Distinguishing Isolated Majorana Fermions from Andreev Bound States. *Phys Rev B* (2019) 99:155159. doi:10.1103/PhysRevB.99.155159
40. Ramos-Andrade JP, Pena FJ, Gonzalez A, Avalos-Ovando O, and Orellana PA. Spin-seebeck Effect and Spin Polarization in a Multiple Quantum Dot Molecule. *Phys Rev B* (2017) 96:165413. doi:10.1103/PhysRevB.96.165413
41. Zeng QB, Chen S, and Lu R. Fano Effect in an Ab Interferometer with a Quantum Dot Side-Coupled to a Single Majorana Bound State. *Phys Lett A* (2016) 380:951. doi:10.1016/j.physleta.2015.12.026

Conflict of Interest: The authors declare that the research was conducted in the absence of any commercial or financial relationships that could be construed as a potential conflict of interest.